Intraseasonal Oscillations in the Mid-Latitudes: Observations, Theory, and GCM Results

Michael Ghil[1], Dmitri Kondrashov[2], François Lott[3] and Andrew W. Robertson[4]

[1] Atmospheric Sciences Dept. & IGPP, UCLA, and Dépt. Terre–Atmosphère–Océan & LMD, ENS, Paris
[2] Atmospheric Sciences Dept. & Institute of Geophysics and Planetary Physics, UCLA
[3] Laboratoire de Météorologie Dynamique du CNRS, IPSL, Paris
[4] International Research Institute for Climate Prediction, Palisades, NY

Abstract

We examine in this paper the role that oscillatory interactions between the jet stream and Northern Hemisphere (NH) mountain ranges play in the low-frequency variability (LFV) of the mid-latitude atmosphere. The basic observational evidence for intraseasonal oscillations in the NH extratropics is reviewed, along with the results of a hierarchy of models—from the simplest to full GCMs—that explain these observations as arising from an oscillatory topographic instability.

We next report on recent reanalysis results that allow one to explicitly connect large-scale flow-pattern changes with oscillatory changes in atmospheric angular momentum, which appear to be driven by mountain-torque changes. An intermediate model with fairly realistic climatology and LFV is used to establish a relationship between these oscillatory circulation changes and the model's Markov chain of multiple flow regimes. We return to the reanalysis results to show that certain phases of the regional mountain-torque oscillations are fair predictors of flow-pattern changes up to 15 days in advance. Open questions are emphasized at the end.

1. Introduction

Intraseasonal time scales range from the deterministic limit of atmospheric predictability, of about 10 days, up to a season, say 100 days. They occupy a window of overlap between short climatic time scales and low-frequency variability intrinsic to the atmosphere. These time scales are of particular importance to extended-range weather prediction. There are two complementary ways of describing low-frequency atmospheric variability in the extratropics: i) *episodic*, via multiple weather regimes (Reinhold and Pierrehumbert, 1982) or planetary flow regimes (Legras and Ghil, 1985), and (ii) *oscillatory*, via broad-peak, slowly modulated oscillations (Ghil *et al.*, 1991a, and references therein). Ghil and Robertson (2002) have recently reviewed these two approaches — which they dubbed the "particles" and "waves" approach, respectively — and their complementarity. We expand here upon recent results using the oscillatory approach, the connections with the episodic one, and their implications for predictability.

The plan of the paper is the following. In Section 2 we review earlier results on intraseasonal oscillations, both observational and theoretical. Simulations of the mid-latitude oscillations using a general circulation model (GCM) in which tropical oscillations were absent are recalled in Section 3 and their spatio-temporal pattern is compared with that predicted by simpler models. We present recent observational results using a 40-year reanalysis in Section 4; these results highlight the role of mountain torques in driving large-scale oscillations in the flow. The complementarity between the episodic and oscillatory approach to low-frequency variability is explored further in Section 5, using an intermediate model with fairly realistic behavior. In Section 6, we combine these two approaches in showing the predictive skill of mountain torques up to 15 days ahead. A summary of results and a list of open questions appear in Section 7.

2. Extratropical oscillations: observations and theory

A convenient indicator of intraseasonal variability is the global atmospheric angular momentum (AAM). Variations in global AAM and in the length of day are highly correlated with each other on intraseasonal time scales; both quantities exhibit spectral peaks with periods near 40 and 50 days (Dickey *et al.*, 1991), among others. Essentially, the Earth-atmosphere system is closed with respect to angular momentum exchanges on this time scale, except for the well-known tidal effects of the Sun and Moon, which can be easily computed and eliminated. Once this is done, what remains is the following: when the mid-latitude westerly winds pick up, or the tropical easterlies slow down, the solid earth slows down in its rotation, and the length of day increases; hence the high positive correlation between the latter and AAM.

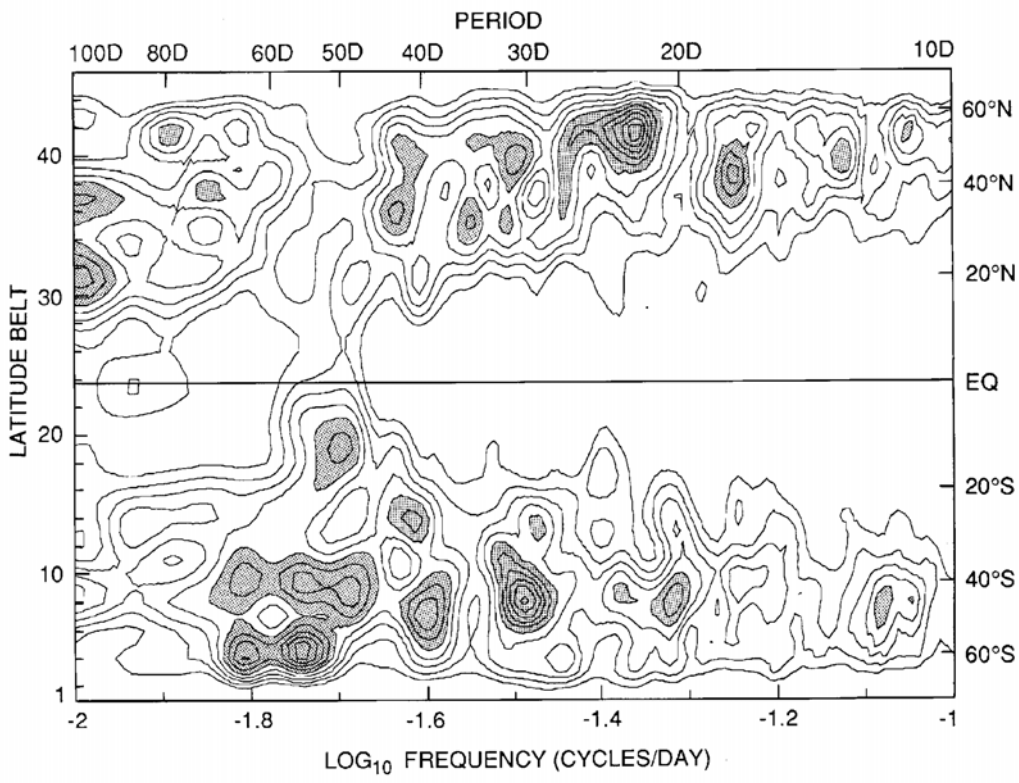

Figure 1: Latitude-frequency dependence of observed AAM variance, as shown by a contour plot of power spectral density for the 46 equal-area belts numbered from south to north. The power in each belt has been multiplied by the frequency; units are angular momentum squared [(1/600) ms]^2. The contour interval is 5.0, with contours starting at 20.0; values over 40.0 are shaded. Reproduced from Dickey et al. *(1991), with the permission of the American Geophysical Union.*

The latitude-frequency dependence of observed AAM variance is shown in Fig. 1, averaged over twelve years and all seasons. It is clear from the figure that the 50-day peak is largely associated with AAM fluctuations in the tropics, which dominate the global AAM. The 40-day peak, however, appears to be associated primarily with variations in the strength of the mid-latitude westerlies: such a peak appears both in the Northern Hemisphere (NH) and in the Southern Hemisphere. The amplitude of the 40-day oscillations in zonal winds is known, however, to be largest during boreal winter, when the winds are strongest in the NH (Weickmann *et al.,* 1985; Ghil and Mo, 1991a; Strong *et al*., 1993, 1995), and we shall thus concentrate here on the longer data sets and more detailed modeling studies for the NH.

The extent to which the tropical and NH oscillations are independent phenomena or influence each other is still the subject of active debate. Madden and Julian (1971, 1972) discovered the tropical oscillation in zonal winds and tropical convection over the equatorial Pacific and progress in its study is documented throughout

these *Proceedings*. The upshot is that intraseasonal variability in the tropics is very rich and its origins are not well understood to this day.

Extratropical oscillations have been found in observed NH planetary-scale circulation anomalies with periods of 20–70 days (Branstator, 1987; Kushnir, 1987; Ghil and Mo, 1991a; Plaut and Vautard, 1994). There is some evidence that the mid-latitude circulation over the North Pacific is correlated to convective anomalies associated with the tropical oscillation (Weickmann *et al.*, 1985; Lau and Phillips, 1986; Higgins and Mo, 1997). On the other hand, Dickey *et al.* (1991) and Ghil and Mo (1991a) found the extratropical mode to be often independent of, and sometimes to lead the tropical one. Upper-level potential vorticity anomalies are known to propagate from the mid-latitudes into the tropics, associated with northwest-to-southeast (NW–SE) tilting troughs (Liebmann and Hartmann, 1984). They are accompanied by cold surges and can cause episodes of intense tropical convection that appear to be related to the intraseasonal oscillation in the tropics (Lau and Li, 1984; Hsu *et al*., 1990).

We pursue here a threefold story: (i) how a hierarchy of models can be used to formulate and test the hypothesis that an intrinsic oscillatory mode of the NH extratropics is associated with the interaction of the jet stream with mid-latitude mountain ranges; (ii) the connection of this NH intraseasonal oscillation with multiple regimes; and (iii) how this oscillation can be useful in extended-range prediction. Charney and DeVore (1979) formulated the topographic hypothesis for the origin of NH intraseasonal variability. They used a highly idealized "toy" barotropic model to study the interaction between a zonal jet and simple zonal-wavenumber 2 topography. Their model exhibits two stable equilibria for the same strength of the prescribed zonal forcing, which represents the strength of the pole-to-equator temperature contrast.

Figure 2a shows the model's *bifurcation diagram*, with the strength ψ_A of the zonal jet in the model's steady-state solutions plotted against the corresponding strength ψ_A^* of the forcing. The two stable equilibria—marked *Z* and *R*—— are associated with "zonal" (higher AAM) and "blocked" (lower AAM) flow respectively, as illustrated in Fig. 2b. The near-zonal solution is close in amplitude and spatial pattern to the forcing jet and is influenced very little by the topography, while the blocked solution is strongly affected by it. In the blocked-flow solution, a ridge is located upstream of the "mountains", similar to the situation during a typical observed West Coast block. This configuration, with a negative zonal pressure gradient on the windward slope of the mountains, corresponds to a negative mountain torque on the atmosphere.

More complex models—both barotropic and baroclinic, with more spatial degrees of freedom than Charney and DeVore's (1979)—have been found to exhibit multiple flow patterns that are similar to those just described, for realistic values of the forcing. The crucial difference in these models is that the equilibria are no longer stable, and the system oscillates around the blocked solution or fluctuates between the zonal and blocked solutions in an irregular way (Legras and Ghil, 1985).

Jin and Ghil (1990) showed that, when a sufficiently realistic meridional structure of the solutions' zonal jet is allowed, the back-to-back *saddle-node bifurcations* of Fig. 2a are replaced by *Hopf bifurcation* and thus transition to finite-amplitude periodic solutions—also called limit cycles — can occur. Eigenanalyses of the unstable equilibria in a higher-resolution barotropic model, as well as its time-dependent solutions, also indicate oscillatory instabilities with intraseasonal (35–50 days) and biweekly (10–15 days) time scales (Strong *et al.*, 1993). Floquet analysis of this model's limit cycles (Strong *et al.*, 1995) confirms that the intraseasonal oscillations that arise in it by oscillatory topographic instability are stronger in winter than in summer, like the NH observed oscillations (Knutson and Weickmann, 1987; Ghil and Mo, 1991a).

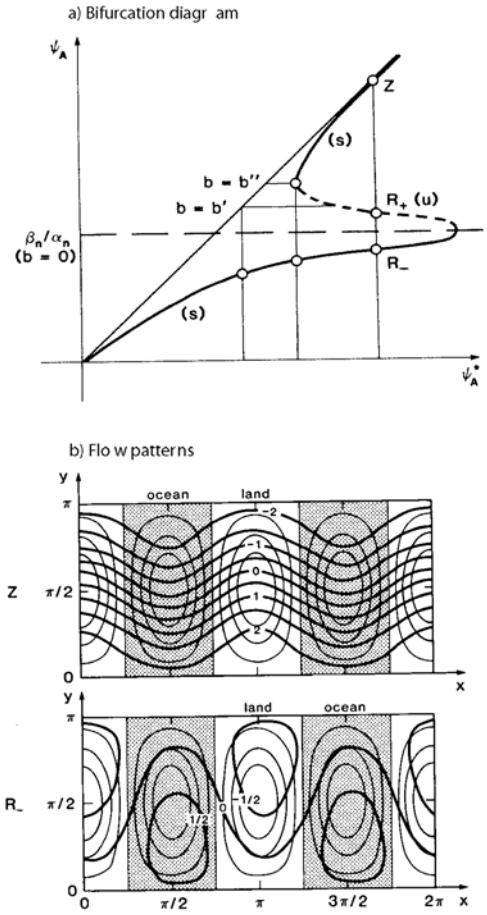

Figure 2: Multiple equilibria of a three-mode quasi-geostrophic model with simplified forcing and topography. (a) Bifurcation diagram showing model response to changes in forcing; see text for the explanation of abscissa and ordinate. The S-shaped bifurcation curve is typical of two back-to-back saddle-node bifurcations *that give rise to two stable solution branches (solid) separated by an unstable one (dashed). (b) Flow patterns of the zonal (upper panel) and blocked (lower panel) equilibria, corresponding to the two stable equilibria* Z *and* R_. *After Charney and DeVore (1979); reproduced from Ghil and Childress (1987), with the permission of Springer-Verlag.*

3. GCM simulations and their validation

Atmospheric GCMs provide a powerful tool for testing the theory of NH extratropical oscillations developed in simpler models. Marcus *et al.* (1994, 1996) made a 3-year perpetual-January simulation with a version of the UCLA GCM that produced no self-sustained Madden-Julian oscillation in the tropics. A robust 40-day oscillation in AAM was found to arise in the model's NH extratropics when standard topography is present. Three shorter runs with no topography produced no intraseasonal oscillation, consistent with a topographic origin for the NH extratropical oscillation in the standard model. The spatial structure of the circulation anomalies associated with the model's extratropical oscillation is shown in Fig. 3, in terms of 500-mb geopotential height composites during the peak (panel a) and quadrature (panel b) phase of the AAM cycle.

The oscillation is dominated by a standing, wavenumber-two pattern, which undergoes tilted-trough vacillation. High values of AAM are associated with low 500-mb heights over the northeast Pacific and Atlantic Oceans (Fig. 3a), and *vice-versa.* This resembles the configuration seen in Charney and DeVore's (1979) simple model (see Fig. 2b here). The GCM's NE–SW tilting phase in Fig. 3a and NW–SE tilting phase in Fig. 3b are strongly reminiscent of the extremes and intermediate phases of the 40-day oscillation that arises by Hopf bifurcation from the blocked equilibrium in the Legras and Ghil (1985) model (M. Kimoto, pers. commun., 1986).

The successive phases of the 28–72-day band-passed fluctuations in 250-mb streamfunction anomalies analyzed by Weickmann *et al.* (1985; see Figs. 7 and 9a–d there) also exhibit good agreement with the evolution of the 40-day oscillation in the work of Marcus and colleagues with the UCLA atmospheric GCM (see Ghil *et al.*, 1991b, for a video clip of the evolution of 500-mb heights, 250-mb streamfunction fields, and sea-level pressures during the atmospheric GCM's 40-day oscillation).

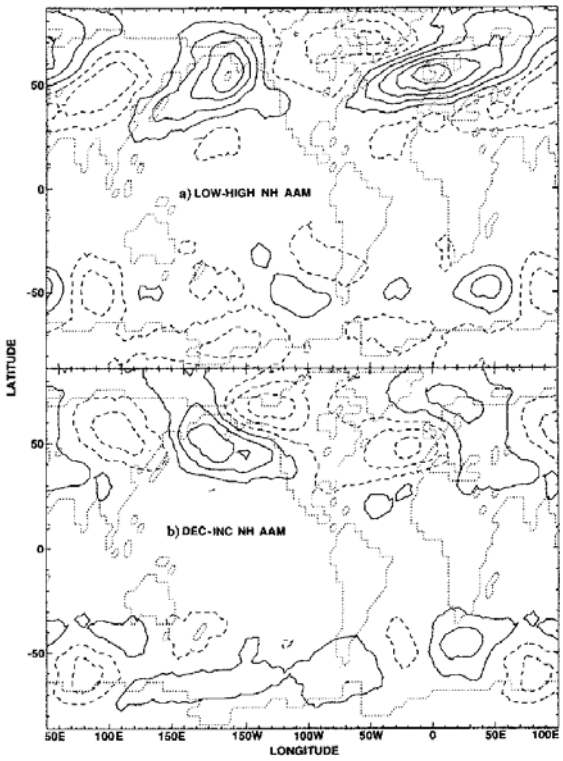

Figure 3: Composite 500-mb maps from the perpetual-January GCM experiment of Marcus et al. *(1996). (a) For days on which the 36-60 day NH extratropical AAM exceeded 1.5 times its rms value; maps for days with a negative (positive) anomaly were added with a positive (negative) sign. (b) Constructed from maps taken 12 days earlier than those included in (a). Contour interval is 20m, and negative contours are dashed. Reproduced from Marcus* et al. *(1996), with the permission of the American Meteorological Society.*

In the GCM, the two centers of action have slightly different frequencies; this gives rise to a long-period modulation (of about 300 days) in the amplitude of the intraseasonal oscillation, similar to that observed by Penland *et al.* (1991) in globally averaged AAM time series. Global correlations with the leading empirical orthogonal functions (EOFs) of the NH extratropical 500-mb height field show NE–SW teleconnection patterns extending into the tropics, in particular into the Indian Ocean, similar to those found in observational studies (Weickmann *et al.*, 1985; Murakami, 1988). The model's zonally averaged latent heating in the tropics exhibits no intraseasonal periodicity, but an oscillation with a period near 40 days is found in cumulus precipitation over the western Indian Ocean, suggesting an extratropical trigger of the 50-day oscillation in the tropics. Madden and Speth (1995; see Fig. 10 there) find that (mostly extratropical) mountain torques do lead (mostly tropical) friction torques and eastward-moving convective systems during the 1987-88 winter singled out already by Dickey *et al.* (1991; their Fig. 16).

Thus the careful analysis of perpetual-January runs with an atmospheric GCM confirms, on the one hand, the topographic origin of the NH 40-day oscillation, originally suggested by simple- and intermediate-model studies (Ghil and Childress, 1987, Sec. 6.4; Jin and Ghil, 1990). On the other, it provides greater realism and spatio-temporal detail, thus permitting a much better confrontation of the theory with the existing observations (Dickey *et al.*, 1991; Ghil and Mo, 1991a).

4. Recent observational results

The height pattern in Fig. 3a is very similar, furthermore, to the extreme-phase patterns obtained from observed data by Lott *et al*. (2003a, b). The NCEP/NCAR reanalysis that spans the 40 years from 1958 to 1997 (Kalnay *et al*., 1996) contains fields of derived quantities, which are not present in the direct observations and which allow one to verify the AAM balance:

$$dM/dt = T_M + T_B, \tag{1}$$

where M is the global AAM, T_M is the mountain torque, and T_B is the frictional torque.

Lott *et al.* (2003a, b) used the daily averages of the surface pressure field p_s, the 700-hPa geopotential heights Z_{700}, and the zonal wind u at the 19 pressure levels given by the analysis, as well as model forecasts of boundary-layer stresses. They found that the AAM balance (1) is closed in the reanalysis to a very good approximation, with a correlation coefficient r = 0.87 between $T_M + T_B$ and dM/dt. Moreover, the global mountain torque T_M is dominated by its NH contribution, between 20° and 90°N.

To focus attention on the intraseasonal (IS) band, the daily series was band-pass filtered with half-power points at 10 and 150 days. Furthermore, a 20–30-day band-pass filter was also used that is very close to unity between 17 and 33 days and is nearly zero outside the 14–50-day band. In the following, all the daily series filtered this way, and sampled every 3 days, will be referred to as the 20–30-day series.

For the NH T_M the 20–30-day series matches very well, in phase and amplitude, the IS series: the correlation between the two is around 0.8. The 20–30-day series accounts typically for 45% of the variance of the IS series (Lott *et al*., 2003a).

Figures 4a–d show composites of hemispheric geopotential heights at 700 hPa that are associated with the 20–30-day NH T_M. These composites are built from Z_{700} maps in the IS band, selected when the 20–30-day NH mountain torque exhibits a local extremum that exceeds in amplitude a given threshold. At zero lag for instance (Fig. 4a), the composite is the sum of the IS Z_{700} maps corresponding to dates when the NH T_M exceeds the prescribed threshold, minus the sum of the IS Z_{700} maps corresponding to dates when the NH T_M has a local minimum that is below minus that threshold. The composite map is then divided by the number N_c of extrema in NH T_M that where selected to build the composites. At non-zero lag, the composites are built using the same procedure, but with maps corresponding to dates at fixed lag from the N_c local extrema identified before in the 20–30-day NH T_M. The threshold value is, of course, arbitrary, and the number N_c of cycles included in a given composite decreases when the threshold increases. The composite spatial patterns are not sensitive, however, to moderate changes in the threshold. The threshold value used in Figure 4 is 17 H $\approx 1.7\sigma_T$, where σ_T is the standard deviation of the IS NH mountain torque; in this case, N_c is near 80.

In Figs. 4a–d, only half a cycle is shown, since the anomaly patterns in the second half are similar in shape and of opposite sign to those in the first half. Areas that equal or exceed a 95% Monte-Carlo test for the significance of the anomalies are shaded. The test used an ensemble of 100 surrogate anomaly composite maps, constructed by averaging N_c height anomaly maps chosen at random.

At zero lag with respect to the extrema of T_M (Fig. 4a), the composite essentially shows a low west of the Rockies and an east–west dipole northwest of the Himalayas. These two features correlate well with large torques over the Rockies and the Himalayas, respectively (Lott *et al*., 2003b), and give rise to a large NH torque according to Fig. 5 below.

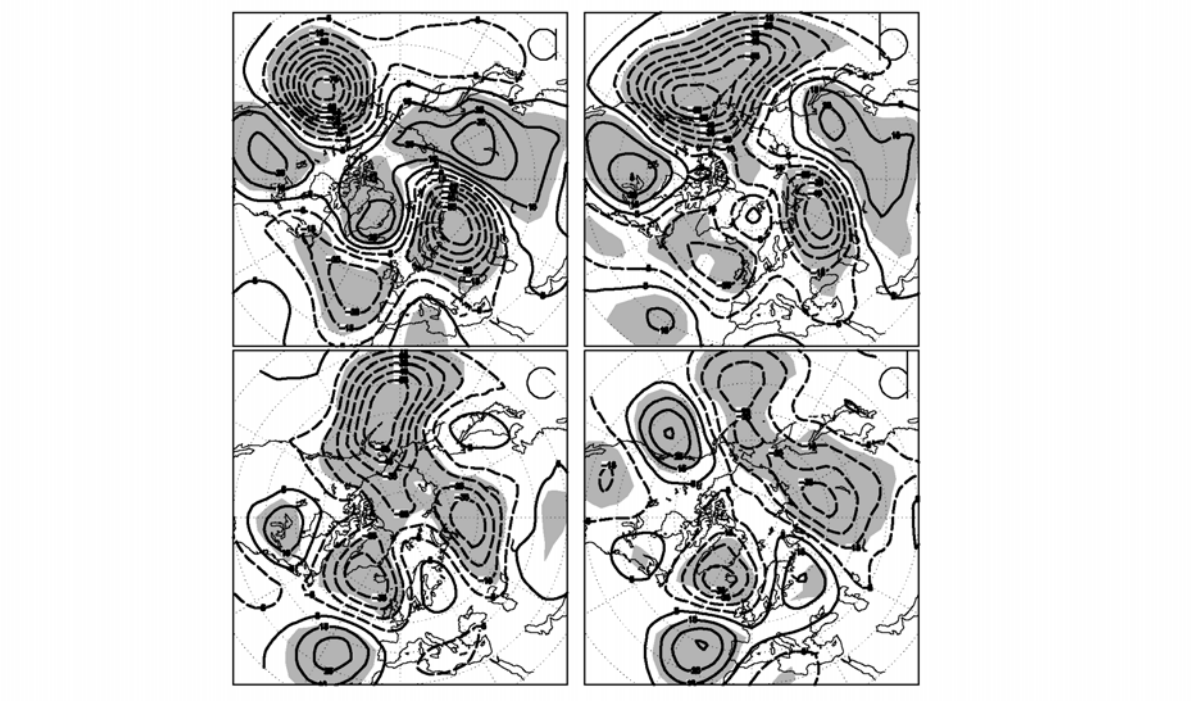

Figure 4: Composite anomalies of Z_{700} from the IS time series, keyed to the 20–30-day NH mountain torque: (a) 0-day lag; (b) 3-day lag; (c) 6-day lag; and (d) 9-day lag. Contour interval: 10 m; positive values, heavy solid; negative values, heavy dashed; 95% confidence shaded; continental contours are light solid. The days for each composite cycle are counted from the local extremum of the 20–30-day NH T_M *for that cycle. Reproduced from Lott* et al. *(2003a), with the permission of the American Meteorological Society.*

At 3-day lag (Fig. 4b) the anticyclonic anomalies have decayed in area, while the cyclonic anomalies have grown. At 6-day lag (Fig. 4c), *i.e.* at the time of approximate quadrature with the NH torque, the patterns are predominantly cyclonic; they correspond to positive zonal wind anomalies in the mid-latitudes. At that time, the zonal average of the Z_{700} composites (not shown) is nearly everywhere negative in the NH; this average also decreases monotonically from near 0 m at 20°N to a minimum of –25 m near 65°N. At 9-day lag (Fig. 4d), east–west dipoles start to build-up over the Rockies and along the western flank of the Himalayas; their polarity is opposite to the pattern in Fig. 2 in Lott *et al*. (2003a) and thus results in a negative torque.

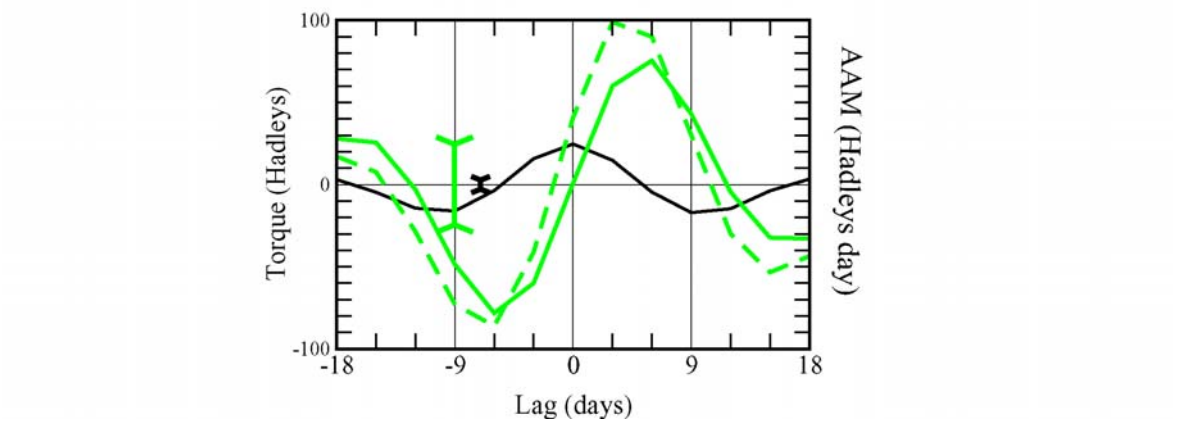

Figure 5: Composites of different terms in the AAM budget during the composites cycle illustrated in Fig. 4. Intraseasonal Northern Hemisphere mountain torque (IS NH T_M*) is the black solid line; integral of IS NH* T_M *(green solid); and global IS AAM (green dashed). Units for the global atmospheric angular momentum,* M*, are in Hadley-day: 1 Hd =* $8.64*10^{22}$ kgm^2s^{-1}*; units for the mountain torque are in Hadleys: 1 H =* 10^{18} kgm^2s^{-2}*. The vertical black bar and the vertical green bar indicate the 95% confidence interval of a Monte-Carlo test for the torque and for the global AAM, respectively. Reproduced from Lott* et al. *(2003a), with the permission of the American Meteorological Society.*

To corroborate that the patterns in Fig. 4 are associated with substantial changes in AAM that are driven by the NH T_M, Fig. 5 shows composites of the different terms of the AAM budget. They are built from the IS series of M and NH T_M, using the N_c days selected in Fig. 4. The 95% confidence levels are from a Monte-Carlo test, constructed as for the Z_{700} composites, but using the IS NH T_M and AAM series to compute surrogate averages of these quantities. The NH mountain torque composite (black solid line in Fig. 5) has a maximum of 24 H at 0-day lag, surrounded by two minima near –20 H at –9-day and +9-day lag, respectively. These three extrema are significant at the 95% level. They are also quite substantial when compared to the standard deviation σ_T of the IS NH T_M, $\sigma_T \approx 10$ H.

The AAM response to be expected from this NH T_M composite can be evaluated by integrating the mountain torque composite in time (solid green line in Fig. 5, where it is expressed in Hadley-day). This response is also quite substantial; it exhibits two extrema of opposite sign and equal to approximately ±75 Hd, while the IS M standard deviation σ_M is about 100 Hd. The green dashed line in Fig. 5 denotes the composite of the IS M, and behaves very much like the integral of the composite of NH T_M.

Over the Pacific sector, our coherent large-scale 20–30-day circulation patterns are consistent with those obtained by more direct methods (Branstator, 1987; Kushnir, 1987; Ghil and Mo, 1991a). These authors have shown that during certain winters, NH variability in the Pacific can be dominated by large-scale oscillations in this band. At least the nonzonal part of the composites in Fig. 4 has much in common with the Branstator–Kushnir oscillation, in which a large circulation anomaly over the Pacific propagates slowly westward. Note as well that this westward propagation is another indication that the sequence of maps in Fig. 4 is not primarily related to tropical oscillations, since the MJO propagates eastward (Madden and Julian, 1994).

Over the Atlantic sector the anomaly patterns in Figs. 4a and 4d are well correlated with the North-Atlantic Oscillation (NAO), as defined by Wallace and Gutzler (1981). The power spectrum of this mode is known to have some power at periodicities near 30 days (Plaut and Vautard, 1994). The latter authors have shown that the NAO-mode is also associated with anomalies originating over northeastern Europe. It is not surprising, therefore, to find it linked with the mountain torque of the Himalayas (cf. Fig. 2 in Lott *et al*., 2003a).

5. Connection to multiple regimes

Kondrashov *et al*. (2003) recently examined the connection between intraseasonal oscillations and multiple regimes for the NH mid-latitude circulation in the quasi-geostrophic (QG) model of Marshall and Molteni (1993). This intermediate-complexity model is based on the QG equations for the conservation of potential vorticity and it has 3 levels in the vertical (hence we refer to it as the QG3 model) and a T21 truncation in the horizontal. Using fairly realistic topography, land-sea contrast and residual forcing (see Corti *et al*., 1997), this QG3 model produces respectable climatology and low-frequency variability.

Kondrashov *et al*. (2003) analyzed a 54,000-day long perpetual-winter integration of this model from the point of view of coarse-graining its phase space (Ghil, 1987; Haines, 1994; Ghil and Robertson, 2002). The first step in this approach is to verify the presence of clusters in the data set that correspond to multiple weather regimes. These represent, in principle, regions of higher probability density function (PDF) on the model's attractor.

The clusters were obtained by using two distinct methods, the *k*-means method of Michelangeli *et al*. (1995) and the Gaussian mixture modeling of Smyth *et al*. (1999), in the subspace of the four leading empirical orthogonal functions (EOFs) of the model simulation's 500-hPa streamfunction field. The results were optimized by comparing the two methods and yielded four NH clusters. The model clusters resemble NAO^+ and NAO^-, that is the zonal and blocked phases of the North Atlantic Oscillation (NAO), and AO^+ and AO^-,

that is the high- and low-index phases of the Arctic Oscillation (AO). Three of these clusters (NAO^+ and NAO^-, as well as AO^+) appear in Fig. 6.

The four regimes that are best supported by synoptic experience, as well as statistical analysis of the upper-air data for the past half-century, are the zonal and blocked phases of westerly flow in the Atlantic–Eurasian and Pacific–North-American (PNA) sector, respectively (Cheng and Wallace, 1993; Smyth *et al*., 1999; Ghil and Robertson, 2002). The NH annular modes (Wallace, 2000) are only statistically annular: they represent a redistribution of mass between the poles and subtropics, but any given "sloshing" event is sectorial; hence the correlation between the subtropical highs over the North Atlantic and the North Pacific is quite low. Both the AO and NAO indices are, however, dominated by Arctic sea-level pressure variations, and hence the NAO and AO are highly correlated in observations. Seeing the PNA-sector patterns replaced in our classification by the hemispheric AO^+ and AO^- ones is thus not too surprising: the latter two overlap largely in the Atlantic–Eurasian sector with NAO^+ and NAO^-, respectively, from which they differ mostly by very strong centers of action in the PNA sector (see again Fig. 6).

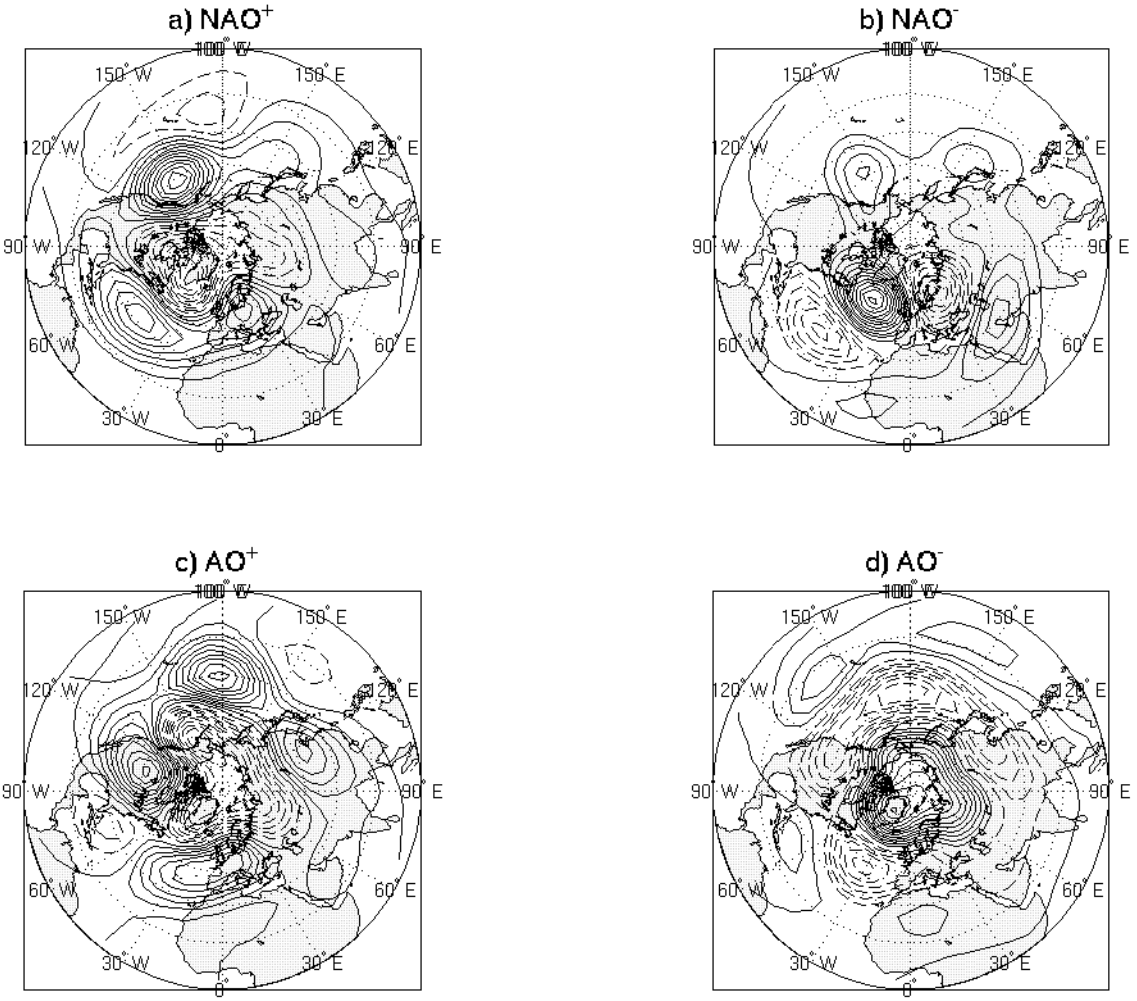

Figure 6: Mixture model centroids computed in a subspace spanned by d = *3 empirical orthogonal functions (EOFs) when using* k = *4 gaussian components in the mixture. The centroids are represented by streamfunction anomaly maps at 500 hPa: a)* NAO^+*; b)* NAO^-*; c)* AO^+*; and d)* AO^-*. Negative contours are dashed and land masses are shaded; twenty contour levels between maximum and minimum values are used, with the following intervals (in* 10^6 m^2 s^{-1}*): a) 1.1, b) 0.8, c) 0.8, and d) 1.1.*

The second step in the multiple-regime approach to low-frequency variability is to determine the Markov chain of transitions between regimes (Ghil, 1987; Mo and Ghil, 1988; Molteni *et al*., 1990; Kimoto and Ghil, 1993b). In the language of dynamical systems theory, this corresponds to a particular representation of the "skeleton of the attractor", which we take here to mean its most interesting and robust part.

One robust transition cycle, $NAO^+ \rightarrow AO^+ \rightarrow NAO^- \rightarrow NAO^+$, is significant at the 95% level in the subspace spanned by the model's three leading EOFs. Direct transitions between the opposite phases of the AO are significantly unlikely, at the 95% level, independently of the cluster size used in deriving the Markov chain.

Likewise a direct transition from the zonal NAO^+ to the blocked NAO^- is quite unlikely. The model results of Kondrashov *et al*. (2003) thus strongly support the nonlinear origin of these well-known NH regimes, already established in observational data by Mo and Ghil (1988) and Kimoto and Ghil (1993b).

Kondrashov *et al*. (2003) further refined the Markov chain representation of regime transitions by finding the preferred transition paths in a three-dimensional (3-D) subspace of the model's phase space. The angular PDF of the regime exits that correspond to these preferred transitions have one or, sometimes, two fairly sharp maxima (not shown). These angular PDF maxima are, in most cases, not aligned with the line segments between regime centroids in phase space and might point to heteroclinic or homoclinic connections between unstable equilibria in the model's phase space. D. Kondrashov (pers. commun., 2003) obtained similar results in NH observational data .

A complementary way of describing the skeleton of our model's attractor is by using the least-unstable periodic orbits (Ott *et al*., 1994, and references therein). Kondrashov *et al*. (2003) carried out multi-channel singular-spectrum analysis (M-SSA) of the 54,000-day-long model trajectory (Plaut and Vautard, 1994; Ghil *et al*., 2002) in the same subspace as for the Markov chain. Two pairs of oscillatory modes are statistically significant at the 95% level, although they capture only a small fraction of the variance (about 10% of the combined variance of spatial PCs 2 and 3). These two modes have periods of 37 days and 19 days.

To analyze the behavior of these oscillations, Kondrashov *et al*. (2003) used composite maps keyed to the phases of the oscillation. For the 37-day oscillation (see Fig. 6), the cycle of regime transitions $NAO^+ \rightarrow AO^+ \rightarrow NAO^-$ is easily identified. After passing through the NAO^+ and AO^+ phases, however, the next phase resembles the Pacific–North-American (*PNA*) pattern, before reaching the NAO^- phase. Thus the Markov-chain cycle $NAO^+ \rightarrow AO^+ \rightarrow NAO^- \rightarrow NAO^+$ appears embedded in the 37-day oscillation.

There is a certain similarity between some phases of the 37-day oscillation and certain phases of the westward-propagating Branstator (1987)–Kushnir (1987) wave; see especially Fig. 5 of Branstator (1987), as well as Dickey *et al*. (1991), Ghil and Mo (1991a), and Plaut and Vautard (1994). There are also marked differences, however, such as the 37-day period here *vs.* that wave's period of 23–25 days, and the very pronounced features of the oscillation in the North-Atlantic–European sector. A video loop (see http: //www.atmos.ucla.edu/tcd), based on 100 composite maps of the cycle, makes it clear that it is mainly a standing oscillation, with occasional northeastward propagation of certain features. In particular it shows strong interaction between the Rockies, on the one hand, and a low and a high that switch places in a counterclockwise fashion between lying upstream and downstream of this mountain range, on the other. The period and standing features of this oscillation, as well as its interaction with the Rockies, resemble certain characteristics of the oscillatory topographic instability of Ghil and colleagues (Legras and Ghil, 1985; Ghil, 1987; Ghil and Mo, 1991a; Ghil *et al*., 1991a; Ghil and Robertson, 2002; see Sections 2 and 3, as well as Fig. 3, in the present paper).

Legras and Ghil (1985) highlighted the slowing down of trajectories near unstable equilibria. Following this suggestion, Vautard (1990) used trajectory speeds as clustering criteria in observational data, while

Mukougawa (1988) and Vautard and Legras (1988) used them in intermediate models of lesser complexity than the present ones; see also Table 1 in Ghil and Robertson (2002). We want to know, therefore, whether there is a systematic connection between any of the model's regimes and the slow phases of the oscillations described by M-SSA.

To do so, Kondrashov *et al*. (2003) computed the velocity in the reduced phase space spanned by the model's three leading EOFs, along the trajectory of a 37-day oscillation, during a particular 100-day long oscillatory spell. Figures 7a–c display the three velocity components, obtained by differencing the time series for each of the three channels of the reconstructed components (RCs) that capture this oscillation, and Fig. 7d presents the speed. The velocity components are highly periodic with the period of 37 days, while the period of the speed seems to equal half of that. The speed goes through phases of significant acceleration and deceleration, and alternate minima are associated with NAO^- and AO^+.

It is plausible that the statistically significant transitions between the QG3 model's four regimes are related to the presence, at nearby parameter values, of heteroclinic connections between unstable fixed points that lie near the cluster centroids. This conjecture is supported by the results of D'Andrea and Vautard (2001) and D'Andrea (2002), who found a good correspondence between their low-order model's quasi-stationary states and the QG3 model's regimes. The presence of heteroclinic connections is especially likely in the case of the transitions that lean quite noticeably away from the straight-line segments between pairs of centroids.

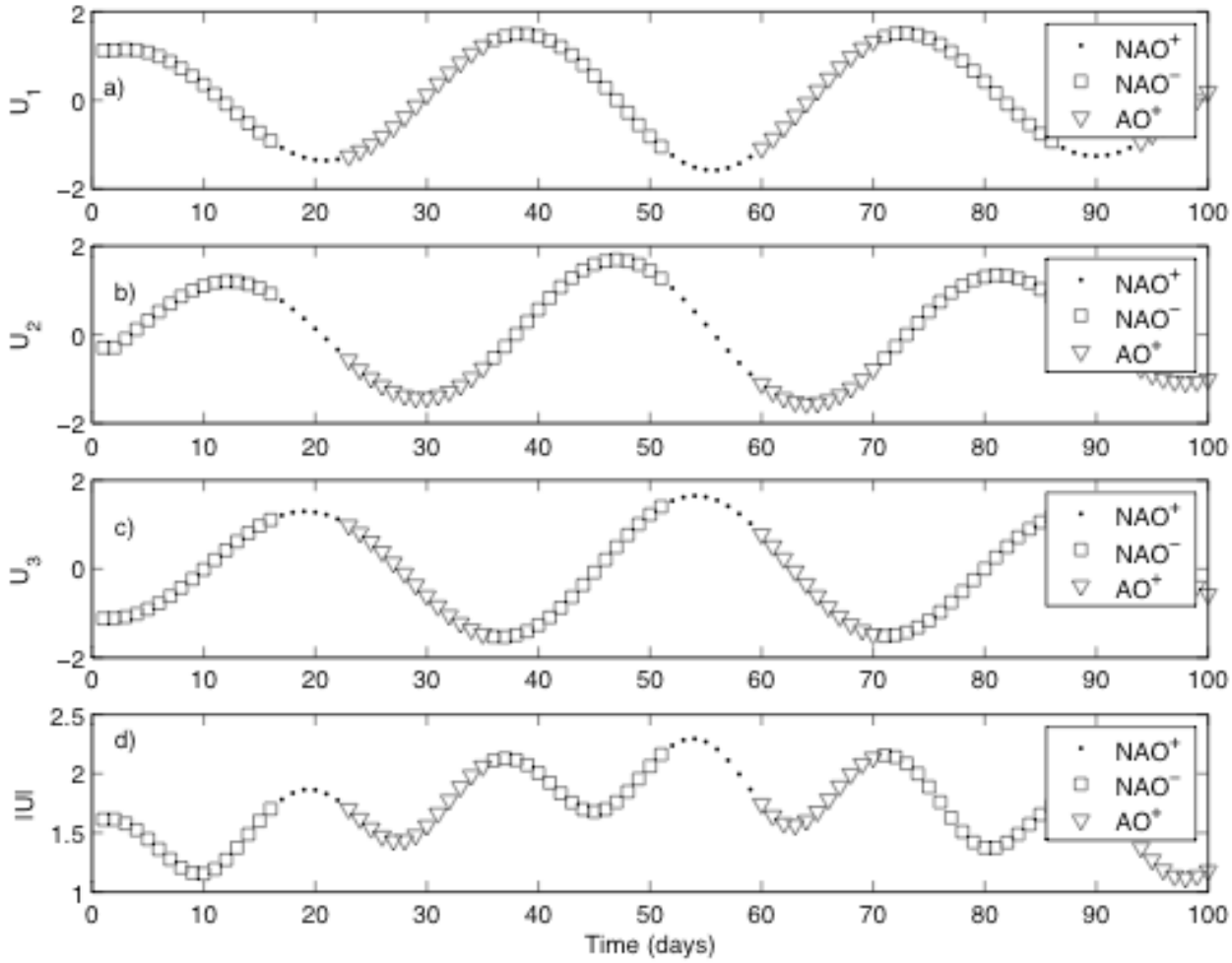

Figure 7: Phase velocity along the trajectory of the 37-day oscillation, in the space of the three leading EOFs, during a 100-day high-amplitude oscillatory spell: (a), (b) and (c) individual velocity components in the direction of EOF 1, 2, and 3, respectively (nondimensional units), and (d) speed. Symbols mark the clusters that the trajectory traverses at that moment.

The strong similarity between the model's closed Markov chain cycle and its 37-day oscillatory mode is another illustration of the interesting, but elusive, relationship between the episodic, multiple-regime description of atmospheric low-frequency variability and the oscillatory one, based on intraseasonal oscillations (Kimoto and Ghil, 1993b; Plaut and Vautard 1994; Ghil and Robertson, 2002; Koo *et al*., 2002). It is quite possible that heteroclinic orbits connect the three regimes of the $NAO^{+} \rightarrow AO^{+} \rightarrow NAO^{-} \rightarrow NAO^{+}$ cycle. Not all three of these need coexist at exactly the same set of parameter values; it suffices that the appropriate parameter values lie close to each other and to those that are most realistic for matching the model behavior to NH atmospheric low-frequency variability.

6. Predictive skill

Koo et al. (2002) already have shown predictive skill for certain phases of the 70-day mode of zonal-flow vacillation in the Southern Hemisphere, with respect to the high-latitude vs. low-latitude regime of mean-jet position (see also Ghil and Robertson, 2002). Given the relationship we discussed so far between NH mountain torques, AAM, and large-scale circulation (see Section 4) and that between flow regimes and intraseasonal oscillations (see Section 5), it is natural to check whether mountain torques cannot help predict, via their effect on AAM oscillations, the onset or break of certain NH weather regimes. Lott *et al*. (2001) reported a preliminary result along these lines, upon which Lott *et al*. (2003b) examined in depth the predictive skill of mountain torques with respect to regime transitions in both the Pacific and Atlantic sector.

For the two Pacific regimes shown in Fig. 8, Lott *et al*. (2003b) computed the probability that the mountain torque in the IS band is positive after a regime episode. In more than 70% of cases, episodes in PAC Regime 1 are preceded for a few days (t = –6, –3 and 0 day) by a positive torque. Conversely, a positive torque precedes the episodes in PAC Regime 2 in less than 35% of cases; this is so for both t = –6 and –3 days.

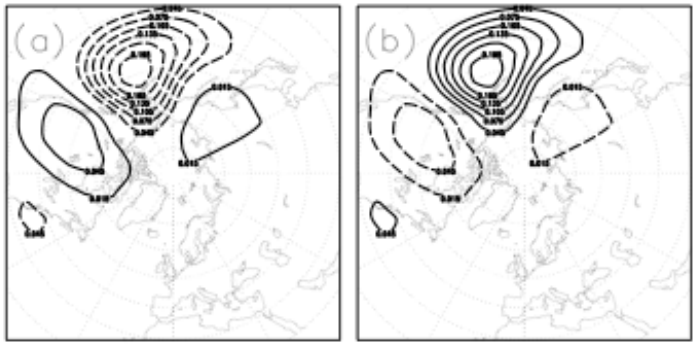

Figure 8: Zonal and blocked regimes over the Pacific sector. The two regimes here strongly resemble contrasting phases of the leading EOF of the NH winter (DJF) variability over the PAC sector.

Lott *et al*. (2003b) evaluated moreover the combined probability P_{PAC} of the two types of above-mentioned circumstances,

$$\text{PPAC}=\text{P}\left(\{\text{TM}>0 \text{ at t after E1}\} \text{ or } \{\text{TM}<0 \text{ at t after E2}\}\right). \quad (2)$$

The most highly significant results are shown in Table 1.

	t(days)						
	T_M	leads		E	leads		
	–15	–6	–3	0	3	6	9
IS NH T_M		66	74	66			39
20–30-d NH T_M		65	71	61		35	32
IS Roc. T_M		71	79	67			
20–30-d Roc. T_M	37	68	69	61		37	37
IS Him. T_M							
20–30-d Him. T_M							

Table 1: Probability (in percent) that a mountain torque T_M *(left column) is either positive* t *days after an episode* E *of PAC Regime 1 or negative* t *days after an episode* E *of PAC Regime 2. IS stands for the intraseasonal, 10–150-day band; 20–30-d stands for the time series filtered by the 20–30-day band pass filter displayed in Fig. 4b of Lott* et al. *(2003a). Only values significant at the 99% level are displayed.*

Row 1 indicates that a strong IS signal in NH mountain torque precedes the Pacific regime episodes at 3, 6 and 9 days. Row 2 confirms that this lead–lag relationship in the IS band largely results from the 20–30-day signal described in Section 4. In this narrower band, a very significant NH T_M signal is present even 15 days prior to the PAC regime episodes. The last two rows in Table 1 show that the above results are essentially the same if one considers the Rockies torque only. This finding is consistent with the Rockies torque having an upstream influence on the PAC regimes.

The fact that mountain torque changes precede PAC regime episodes suggests that the former can be related to the onset of PAC regime events. To address this point, Lott *et al.* (2003b) computed the probability that the mountain torque is positive at the onset of events in PAC Regime 1 and negative at the onset of events in PAC Regime 2. When computed for the NH torque in the IS band, this probability is close to 84%. If the torque value is taken 3 days prior to a PAC regime onset, the probability of the torque having the appropriate sign is still 80%. Again, these links result primarily from an upstream influence of the Rockies, as the two probabilities above are 69% and 77% when evaluated using the Rockies torque in this band.

For the two Atlantic regimes that are characterized by opposite phases of the AO, Lott *et al.* (2003b) found that the mountain torques can participate significantly in their breaks, rather than their onsets (not shown).

7. Perspectives on the NH topographic oscillation

This is a quick summary of what we do and do not know about the intraseasonal oscillations we discussed in this paper, and some considerations about their potential role in medium-range to long-range forecasting.

a. What do we know?

1. The main oscillation we covered appears to be predominantly a *standing wave of zonal wave number* $k = 2$ (see Figs. 2b and 3), as stated by Ghil (1987), based on the results of the simple model of Legras and Ghil (1985). Ghil and Mo (1991a) confirmed this characteristic feature in their analysis of 700-hPa observations and Marcus *et al.* (1994, 1996) did so using the UCLA GCM.
2. The *period of this oscillation* is distinct from the tropical, Madden–Julian one (40 days *vs.* 50 days; see Fig. 1). This was found to be the case by Dickey *et al. (1991)* in AAM data stratified by latitude bands, while Magaña (1993) confirmed it by using both banded AAM and tropical convection (OLR) data.

3. There is little doubt that the presence of *topography is essential* for the instability that gives rise to this oscillation, as demonstrated by Jin and Ghil (1990) in a simple model and by Marcus *et al.* (1994, 1996) in the UCLA GCM; see also Figs. 4 and 5 here.
4. The presence of *higher meridional modes* ($m \geq 2$) in the mean zonal-wind profile is important, as shown by Jin and Ghil (1990) and by Tribbia and Ghil (1990) in a simple and an intermediate model, respectively.
5. *Baroclinic effects*, while present when studying this oscillation in a multi-level or multi-layer model (Keppenne *et al*., 2000), *are secondary*.
6. Dickey *et al.* (1991) detected substantial, though episodic, *equatorward propagation* of wave energy in the banded AAM data, as did Marcus *et al*. (1994, 1996) in their GCM simulation (see also Ghil *et al*., 1991b).
7. This NH mid-latitude oscillation is *stronger in NH winter*, as found by Knutson and Weickmann (1987) and by Ghil and Mo (1991a) in observations and shown by Strong *et al.* (1993, 1995) in an intermediate model.
8. To summarize, this oscillation is *quite robust*, as can be seen from the wealth of evidence recapitulated above. In addition, closely related phenomena appear in the barotropic annulus experiment of Weeks *et al.* (1997) and the associated numerical study of Tian *et al*. (2001).

b. What don't we know?

1. In spite of the convergence of evidence outlined in Section 7a, we still don't know the exact cause of the NH topographic oscillation: the preponderance of evidence favors a local Hopf bifurcation, as worked out in detail by Jin and Ghil (1990). Tribbia and Ghil (1990), however, found a similar oscillation arising from a global nonlinear interaction between several modes.
2. Neither do we know the exact period. All of the work cited in Section 7a — observational, theoretical and numerical, as well as the very recent paper of Kondrashov et al. (2003) — yields a period of 40 days. Lott et al. (2001, 2003a, b), however, find a 20–30 day band (see again Figs. 4 and 5 here).
3. What is the cause of the Branstator (1987)–Kushnir (1987) wave? Branstator and Held (1995) found both unstable and neutral Rossby-Haurwitz modes that share certain observed features of this westward propagating, 23–25-day mode. Both Lott et al. (2003a, b) and Kondrashov et al. (2003) find some of the same westward propagating features in their results, mixed to a certain extent with standing features that resemble the topographic oscillation (see Fig. 4).
4. What is the cause of the Plaut–Vautard (1994) wave over the Atlantic, with its 70-day period? Is it also related to boundary forcing, maybe thermal in the Euro–Atlantic sector vs. the topographic effects in the Pacific–North American sector (see also Keppenne et al., 2000)?
5. What is the cause of the tropical 20–30-day (Ghil and Mo, 1991b) and 40–50-day oscillations? Zhao and Ghil (1991) have provided a plausible explanation for the former but the rest of the papers presented at this workshop provide a still confused picture for the latter.
6. How do the tropical and mid-latitude oscillators interact? Given the closeness of the periods and the various ways of exchanging energy and AAM fluxes between the tropics and the extratropics, it is fairly surprising that no resonance, nor phase-locking occur. What are the synoptic aspects of the interaction, in particular those that inhibit, rather than enhance the interaction?

7. The intraseasonal SH oscillations are much less well studied than the tropical and NH ones. Dickey et al. (1991) found strong peaks at 17, 31 and 48 days in the banded AAM data they studied, and Ghil and Mo (1991b) also found significant 23- and 40-day oscillations in their 500-hPa data. Koo and Ghil (2002) and Koo et al. (2002) explored connections between zonal-flow vacillation, with periods of 70 and 135 days, and the high-latitude and low-latitude jet regimes, while Robertson and Mechoso (2003) studied the complementary facets of the Pacific–South American regimes (Mo and Ghil, 1987) and a 40-day oscillation.

c. *Practical applications to long-range forecasting (LRF)*

1. It is well known by now, following on the work of J. G. Charney, C. E. Leith, E. N. Lorenz, P. D. Thompson and many others, that detailed and accurate prediction of atmospheric flows is limited to 10–15 days, at best. So what is predictable, and how accurately, beyond this limit? The fact that a certain amount of variance exhibits periods longer than this limit gives hope, as illustrated by discussions of seasonal-to-interannual climate forecasting (e.g., Ghil and Jiang, 1998).

2. How can one best predict these recurring features, given the large amount of noise in which they are buried? In short-range prediction detailed numerical models have now been outperforming statistical methods for a long time (Tribbia and Anthes, 1987; Kalnay, 2002), but this is not yet the case in seasonal-to-interannual prediction. Does the only road to LRF lead through greater numerical model resolution and related improvements, i.e., is dynamical forecasting the only hope? Statistical methods by themselves have clear limitations, too, but a judicious combination of the two into a hybrid scheme might outperform single forecasts and even ensemble forecasts. The latter try to bring in some statistics through the Monte Carlo approach (Leith, 1974). Another, complementary way might be to use a statistical forecast of the periodic components of LFV as nudging of a dynamical forecast, whether a single or an ensemble forecast.

Acknowledgments.

It is a pleasure to thank collaborators over many years in the study of mid-latitude intraseasonal oscillations and the role of topography therein; their names appear in numerous references. The opportunity provided by Tim Palmer and the ECMWF to present a review of recent results is greatly appreciated. Our work on this topic has been supported by NSF Grant ATM-0082131 (MG and DK) and DOE Grant DE-FG03-01ER63260 (AWR).

References

Branstator, G. W., 1987: A striking example of the atmosphere's leading traveling pattern. *J. Atmos. Sci.*, **44**, 2310–2323.

Branstator, G., and I. M. Held, 1995: Westward propagating normal modes in the presence of stationary background waves, *J. Atmos. Sci*., **52**, 247–262.

Corti, S., F. Molteni and T. N. Palmer, 1999: Signature of recent climate change in frequencies of natural atmospheric circulation regimes. *Nature*, **398**, 799–802.

Charney, J. G., and J. G. DeVore, 1979: Multiple flow equilibria in the atmosphere and blocking. *J. Atmos. Sci*., **36,** 1205–1216**.**

Cheng, X., and J.M. Wallace, 1993: Cluster analysis of the Northern Hemisphere wintertime 500-hPa height field: Spatial patterns. *J. Atmos.*, **50**, 2674–2696.

Corti, S., A. Giannini, S. Tibaldi, and F. Molteni, 1997: Patterns of low-frequency variability in a three-level quasi-geostrophic model, *Clim. Dyn.*, **13**, 883–904.

D'Andrea, F., and R. Vautard, 2001: Extratropical low-frequency variability as a low-dimensional problem. Part I: A simplified model, *Q. J. R. Meteorol. Soc.*, **127**, 1357–1374.

D'Andrea, F., and R. Vautard, 2002: Extratropical low-frequency variability as a low-dimensional problem. Part II: Stationarity and stability of large-scale equilibria, *Q. J. R. Meteorol. Soc.*, **128**, 1059–1073.

Dickey, J. O., M. Ghil, and S. L. Marcus, 1991: Extratropical aspects of the 40-50 day oscillation in length-of-day and atmospheric angular momentum. *J. Geophys. Res.*, **96**, 22643–22658.

Ghil, M., 1987: Dynamics, statistics and predictability of planetary flow regimes, *Irreversible Phenomena and Dynamical Systems Analysis in the Geosciences*, C. Nicolis and G. Nicolis (Eds.), D. Reidel, Dordrecht/Boston/Lancaster, pp. 241–283.

Ghil, M., and S. Childress, 1987: *Topics in Geophysical Fluid Dynamics: Atmospheric Dynamics, Dynamo Theory and Climate Dynamics,* Springer-Verlag, New York, 485 pp.

Ghil, M., and N. Jiang, 1998: Recent forecast skill for the El Niño/Southern Oscillation. *Geophys. Res. Lett.,* **25**, 171–174.

Ghil, M., and K. C. Mo, 1991a: Intraseasonal oscillations in the global atmosphere. Part I: Northern Hemisphere and tropics. *J. Atmos. Sci.*, **48**, 752–779.

Ghil, M., and K. C. Mo, 1991b: Intraseasonal oscillations in the global atmosphere. Part II: Southern Hemisphere. *J. Atmos. Sci.*, **48**, 780–790.

Ghil, M., and A. W. Robertson, 2002: "Waves" vs. "particles" in the atmosphere's phase space: A pathway to long-range forecasting? *Proc. Natl. Acad. Sci.,* **99** *(Suppl. 1),* 2493–2500.

Ghil, M., and R. Vautard , 1991: Interdecadal oscillations and the warming trend in global temperatures time series, *Nature*, **350**, 324–327.

Ghil, M., M. Kimoto, and J. D. Neelin, 1991a: Nonlinear dynamics and predictability in the atmospheric sciences, *Rev. Geophys.,* **29,** *Supplement* (U.S. Nat'l Rept. to Int'l Union of Geodesy & Geophys. 1987–1990), pp. 46–55.

Ghil, M., S. L., Marcus, J. O. Dickey, and C. L. Keppenne, 1991b: *AAM the Movie*. NTSC videocassette AVC-91-063, Caltech/NASA Jet Propulsion Laboratory, Pasadena, CA 91109 [available also from M. Ghil upon request].

Ghil M., R. M. Allen, M. D. Dettinger, K. Ide, D. Kondrashov, M. E. Mann, A. Robertson, A. Saunders, Y. Tian, F. Varadi, and P. Yiou (2002). Advanced spectral methods for climatic time series. *Rev. Geophys.,***40**(1), pp. **3**.1–**3**.41, 10.1029/2000GR000092.

Haines, K., 1994: Low-frequency variability in atmospheric middle latitudes. *Surveys Geophys.*, **15**, 1–61.

Higgins, R. W., and K. C. Mo, 1997: Persistent North Pacific anomalies and the tropical intraseasonal oscillation. *J. Climate*, **10**, 223–244.

Hsu, H. H., B. J., Hoskins, and F.-F. Jin, 1990: The 1985-86 intra-seasonal oscillation and the role of topographic instabilities. *J. Atmos. Sci.*, **47**, 823–839.

Jin, F.-F., and M. Ghil, 1990: Intraseasonal oscillations in the extratropics: Hopf bifurcation and topographic instabilities. *J. Atmos. Sci.*, **47**, 3007–3022.

Kalnay, E., 2002: *Atmospheric Modeling, Data Assimilation and Predictability*, Cambridge Univ. Press, Cambridge, Mass., 341 pp.

Keppenne, C. L., S. Marcus, M. Kimoto, and M. Ghil, 2000: Intraseasonal variability in a two-layer model and observations, *J. Atmos. Sci.,* **57**, 1010–1028.

Kimoto, M., and M. Ghil, 1993a: Multiple flow regimes in the Northern Hemisphere winter. Part I: Methodology and hemispheric regimes, *J. Atmos. Sci.*, **50**, 2625–2643.

Kimoto, M., and M. Ghil, 1993b: Multiple flow regimes in the Northern Hemisphere winter. Part II: Sectorial regimes and preferred transitions, *J. Atmos. Sci.*, **50**, 2645–2673.

Knutson, T. R., and K. M. Weickmann, 1987: 30-60 day atmospheric oscillations: Composite life cycles of convection and circulation anomalies. *Mon. Wea. Rev.,* **115**, 1407–1436.

Kondrashov, D., K. Ide and M. Ghil, 2004: Weather regimes and preferred transition paths in a three-level quasi-geostrophic model, *J. Atmos. Sci.*, in press.

Koo, S., and M. Ghil, 2002: Successive bifurcations in a simple model of atmospheric zonal-flow vacillation, *Chaos*, **12**, 300–309.

Koo, S., A. W. Robertson, and M. Ghil, 2002: Multiple regimes and low-frequency oscillations in the Southern Hemisphere's zonal-mean flow. *J. Geophys. Res.,* 10.1029/2001JD001353.

Kushnir, Y., 1987: Retrograding wintertime low-frequency disturbances over the North Pacific Ocean. *J. Atmos. Sci.*, **44**, 2727–2742.

Lau, K.-M., and M.-T. Li, 1984: The monsoon of East Asia and its global associations — A survey. *Bull. Amer. Meteorol. Soc.*, **65,** 114–125**.**

Lau, K.-M., and T. J. Phillips, 1986: Coherent fluctuations of extratropical geopotential height and tropical convection in intraseasonal time scales. *J. Atmos. Sci.*, **43**, 1164–1181**.**

Leith, C. E., 1974: Theoretical skill of Monte-Carlo forecasts, *Mon. Weather Rev.,* **102**, 409–418.

Legras, B., and M. Ghil, 1985: Persistent anomalies, blocking and variations in atmospheric predictability. *J. Atmos. Sci.*, **42**, 433–47l.

Liebmann, B., and D. L. Hartmann, 1984: An observational study of tropical-midlatitude interaction on intraseasonal time scales during winter. *J. Atmos. Sci.*, **41**, 3333–3350.

Lott, F., A. W. Robertson, and M. Ghil, 2001: Mountain torques and atmospheric oscillations, *Geophys. Res. Lett.*, **28**, 1207–1210.

Lott, F., A. W. Robertson, and M. Ghil, 2003a: Mountain torques and Northern Hemisphere low-frequency variability. Part I: Hemispheric aspects. *J. Atmos. Sci.,* in press.

Lott, F., A. W. Robertson, and M. Ghil, 2003b: Mountain torques and Northern Hemisphere low-frequency variability. Part II: Regional aspects. *J. Atmos. Sci.,* in press

Madden, R. A., and P. R. Julian, 1971: Detection of a 40–50 day oscillation in the zonal wind in the tropical Pacific. *J. Atmos. Sci.*, **28**, 702–708.

Madden, R. A., and P. R. Julian, 1972: Description of global-scale circulation cells in the tropics with a 40–50 day period. *J. Atmos. Sci.*, **29**, 1109–1123.

Madden, R. A., and P. R. Julian, 1994: Observations of the 40–50 day tropical oscillation — A review. *Mon. Wea. Rev*., **122**, 814–837.

Madden, R.A., and P. Speth, 1995: Estimates of atmospheric angular momentum, friction, and mountain torques during 1987-1988. *J. Atmos. Sci.*, **52**, 3681–3694.

Magaña, V., 1993: The 40-day and 50-day oscillations in atmospheric angular momentum at various latitudes, *J. Geophys. Res*., **98**, 10441–10450.

Marshall, J., and F. Molteni, 1993: Towards a dynamical understanding of planetary-scale flow regimes. *J. Atmos. Sci.*, **50**, 1792–1818.

Marcus, S. L., M. Ghil,, and J. O. Dickey, 1994: The extratropical 40-day oscillation in the UCLA General Circulation Model, Part I: Atmospheric angular momentum, *J. Atmos. Sci.*, **51**, 1431–1466.

Marcus, S. L., M. Ghil, and J. O. Dickey, J. O., 1996: The extratropical 40-day oscillation in the UCLA General Circulation Model, Part II: Spatial structure, *J. Atmos. Sci.*, **53**, 1993–2014.

Michelangeli, P.A., R. Vautard, and B. Legras, 1995: Weather regimes: Recurrence and quasi-stationarity. *J. Atmos. Sci.*, **52**, 1237–1256.

Mo, K., and M. Ghil, 1987: Statistics and dynamics of persistent anomalies, *J. Atmos. Sci.*, **44**, 877–901.

Mo, K., and M. Ghil, 1988: Cluster analysis of multiple planetary flow regimes, *J. Geophys. Res.*, **93D**, 10927–10952.

Molteni, F., S. Tibaldi, and T.N. Palmer, 1990: Regimes in the wintertime circulation over northern extratropics. 1. Observational evidence. *Q. J. R. Meteorol. Soc.*, **116**, 31–67.

Murakami, T., 1988: Intraseasonal atmospheric teleconnection patterns during the Northern Hemisphere winter. *J. Climate,* **1**, 117–131.

Mukougawa, H., 1988: A dynamical model of "quasi-stationary" states in large-scale atmospheric motions. *J. Atmos. Sci.*, **45**, 2868–2888.

Ott, E., T. Sauer, and J. A. Yorke (Eds.), 1994: *Coping with Chaos. Analysis of Chaotic Data and the Exploitation of Chaotic Systems.* J. Wiley & Sons, New York/Chichester/Brisbane/Toronto/Singapore, 418 pp.

Penland, C., M. Ghil, and K. M. Weickmann, 1991: Adaptive filtering and maximum entropy spectra, with application to changes in atmospheric angular momentum. *J. Geophys. Res.*, **96**, 22659–22671.

Plaut, G. R., and R. Vautard, 1994: Spells of oscillations and weather regimes in the low-frequency dynamics of the Northern Hemisphere. *J. Atmos. Sci.*, **51**, 210–236.

Reinhold, B. B., and R.T. Pierrehumbert, 1982: Dynamics of weather regimes: Quasi-stationary waves and blocking. *Mon. Wea. Rev.*, **110**, 1105–1145.

Robertson, A. W., and C. R. Mechoso, 2003: Circulation regimes and low-frequency oscillations in the South Pacific sector. *Mon. Wea.Rev*., **131**, 1566–1576.

Smyth, P., K. Ide and M. Ghil, 1999: Multiple Regimes in Northern Hemisphere Height Fields via Mixture Model Clustering. *J. Atmos. Sci.,* **56**, 3704–3723.

Strong, C. M., F.-F. Jin, and M. Ghil, 1993: Intraseasonal variability in a barotropic model with seasonal forcing. *J. Atmos. Sci.*, **50**, 2965–2986.

Strong, C. M., F.-F. Jin, and M. Ghil, 1995: Intraseasonal oscillations in a barotropic model with annual cycle, and their predictability. *J. Atmos. Sci.*, **52**, 2627–2642.

Tribbia, J. J., and R. A. Anthes, 1987: Scientific basis of modern weather prediction, *Science*, **237**, 493–499.

Tribbia, J. J., and M. Ghil, 1990: Forced zonal flow over topography and the 30–60 day oscillation in atmospheric angular momentum, NCAR Tech. Rep. 0501/89-5, National Center for Atmospheric Research, Boulder, Colo.

Vautard, R., 1990: Multiple weather regimes over the North Atlantic. Analysis of precursors and successors. *Mon. Wea. Rev.*, **118**, 2056–2081.

Vautard, R., and M. Ghil, 1989: Singular spectrum analysis in nonlinear dynamics, with applications to paleoclimatic time series. *Physica D*, **35**, 395–424.

Vautard, R., and B. Legras, 1988: On the source of low frequency variability. Part II: Nonlinear equilibration of weather regimes. *J. Atmos. Sci.*, **45**, 2845–2867.

Vautard, R., P. Yiou, and M. Ghil, 1992: Singular-spectrum analysis: A toolkit for short, noisy chaotic signals, *Physica D*, **58**, 95–126.

Wallace, J. M., 2000: North Atlantic Oscillation/annular mode: Two paradigms — one phenomenon. *Quart. J. Roy. Meteor. Soc*., **126**, 791–805.

Wallace, J. M., and D. S. Gutzler, 1981: Teleconnections in the geopotential height field during the Northern Hemisphere winter. *Mon. Wea. Rev.*, **109**, 784-812.

Weickmann, K. M., G. R. Lussky, and J. E. Kutzbach, 1985: Intraseasonal (30-60 day) fluctuations of outgoing longwave radiation and 250 mb streamfunction during northern winter. *Mon. Wea. Rev.*, **113**, 941–961.

Zhao, J.-X., and M. Ghil, 1991: Nonlinear symmetric instability and intraseasonal oscillations in the tropical atmosphere, *J. Atmos. Sci.*, **48**, 2552-2568.